Dalton Transactions

Actinyl-cation interactions: Experimental and theoretical assessment of [Np(VI)O2Cl4]2- and [U(VI)O2Cl4]2-systems.

Journal:	*Dalton Transactions*
Manuscript ID	DT-ART-04-2019-001753.R1
Article Type:	Paper
Date Submitted by the Author:	17-May-2019
Complete List of Authors:	Bjorklund, Jennifer; University of Iowa, Department of Chemistry Pyrch, Mikaela; University of Iowa, Department of Chemistry Basile, Madeline; University of Iowa, Department of Chemistry Mason, Sara; University of Iowa, Chemistry Forbes, Tori; University of Iowa, Department of Chemistry

SCHOLARONE™
Manuscripts

Actinyl-cation interactions: Experimental and theoretical assessment of [Np(VI)O₂Cl₄]²⁻ and [U(VI)O₂Cl₄]²⁻ systems.

Jennifer Bjorklund, Mikaela M. Pyrch, Madeline C. Basile, Sara E. Mason, and Tori Z. Forbes*

University of Iowa, Department of Chemistry, Iowa City, IA, 52242

*corresponding author: tori-forbes@uiowa.edu; 319-384-1320

Abstract

The interaction of the actinyl (AnO_2^{2+}) oxo group with low-valent cations influences the chemical and physical properties of hexavalent actinides, but the impact of these intermolecular interactions on the actinyl bond and their occurrence in solution and solid state phases remain unclear. In this study, we explore the coordination of alkali-cations (Li^+, Na^+, K^+) with the $[NpO_2Cl_4]^{2-}$ coordination complexes using single-crystal X-ray diffraction, Raman spectroscopy, and density functional theory (DFT) calculations and compare to the related uranyl system. Three solid-state coordination compounds ($[Li(12\text{-}crown\text{-}4)]_2[NpO_2Cl_4]$ (**LiNp**), [Na(18-crown-6)H₂O]₂[NpO₂Cl₄] (**NaNp**), and [K(18-crown-6)]₂[NpO₂Cl₄] (**KNp**)) have been synthesized and characterized using single-crystal X-ray diffraction and Raman spectroscopy. Only Li^+ cations interact with the neptunyl oxo in the solid-state compounds and this results in a red-shift of the NpO_2^{2+} symmetric stretch (v_1). Raman spectra of Np(VI) solutions containing lower Li^+ concentrations display a single peak at ~854 cm⁻¹ and increasing the amount of Li^+ results in the ingrowth of a second band at 807 cm⁻¹. DFT calculations and vibrational analysis indicate the lower frequency vibrational band is the result of interactions between the Li^+ cation and the neptunyl oxo. Comparison to the related uranyl system shows similar interactions occur in the solid state, but subtle differences in the actinyl-cation modes in solution phase.

Introduction

The divalent actinyl moiety, $[AnO_2]^{2+}$, is unique to hexavalent actinide elements and an important feature of uranium, neptunium, and plutonium chemistry.[1] This species contains covalent bonds between the hexavalent metal center and two oxygen atoms, which are arranged in a linear fashion to form the dioxo cation.[2, 3] An-O distances within the $[AnO_2]^{2+}$ unit are short (~ 1.78 Å) indicating the formation of a multiple bond. Stability of actinyl cation has been well-documented, with the reported half-life of oxo exchange ranging from 10^3-10^4 hours for U(VI), Np(VI), and Pu(VI) in acidic solutions.[4-9] This molecular fragment dominates the chemistry of hexavalent U, Np, and Pu in aqueous and non-aqueous systems and is the fundamental building unit for solid-state phases.[2, 3, 10-12]

Strong bonding that occurs within the $[AnO_2]^{2+}$ cation results in limited intermolecular interactions to ions and molecules in the second coordination sphere environment. Covalency within the $[AnO_2]^{2+}$ cation decreases the Lewis basicity of the oxo group, essentially passivating it towards additional intermolecular interactions to neighboring cations or H-bond donors.[13] Due to these limited interactions, most of the chemical reactivity targets the equatorial plane and the results in the formation of solid-state structure that are dominated by lower (1-D or 2-D) dimensional topologies.[2, 3, 11, 12] However, weak interactions with the oxo groups may influence redox chemistry, oxo exchange, and chemical reactivity of the actinyl moiety.[13] Therefore it is important to develop an understanding of the extent of these interactions with the actinyl oxo both in solution and solid-state materials.

Within the actinide series, actinyl-cation interactions associated with the uranyl $(UO_2)^{2+}$ moiety is the most well-studied and can provide a starting point for investigations into transuranic (NpO_2^{2+}, PuO_2^{2+}) chemistry. Fortier and Hayton[13] published an in-depth review of uranyl oxo interactions in both solid-state and solution phase and noted that uranyl-cation

2

interactions are relatively rare within discrete coordination complexes. Within non-aqueous systems, the ability of the ligands in the equatorial plane to donate electron density and promote oxo interactions has been explored by Arnold[14-16] and Burns.[17] These types of interactions are less well known for aqueous systems and related solid-state materials. Theury and Masci[18] published a series of uranyl calixarene coordination compounds that contain interactions to Li^+, Na^+, K^+, Rb^+ and Cs^+. Within these compounds, the alkali metal cations are encapsulated within crown ether complexes or the calixarenes themselves, removing the waters of solvation and allowing for additional interactions with the uranyl oxo. In a related systematic study, Danis et al.[19] reported a series of uranyl tetrahalide complexes (UO_2Cl_4; UO_2Br_4) crystallized with alkali-metal (Li^+, Na^+, K^+) crown ether molecules. Within this investigation, Danis *et al.*[19] delineated four types of interactions that occurred between the $[UO_2Cl_4]^{2-}$ or $[UO_2Br_4]^{2-}$ complex and the alkali cations (Figure 1):

Type I – The alkali cation engages with all four halide anions in the equatorial positions through bidentate coordination on either side of the molecule.

Type II– Only two halide anions interact with the alkali cation through a monodentate coordination on opposite sides of the molecule.

Type III – Interactions occur through two halide anions and the oxo group of the uranyl cation.

Type IV – The alkali cation engages solely with the oxo groups of the uranyl cation. Overall, Danis et al.[19] observed a propensity to form Type I and II interactions, although a rare oxo interaction (Type IV) was observed in the case of Li^+.
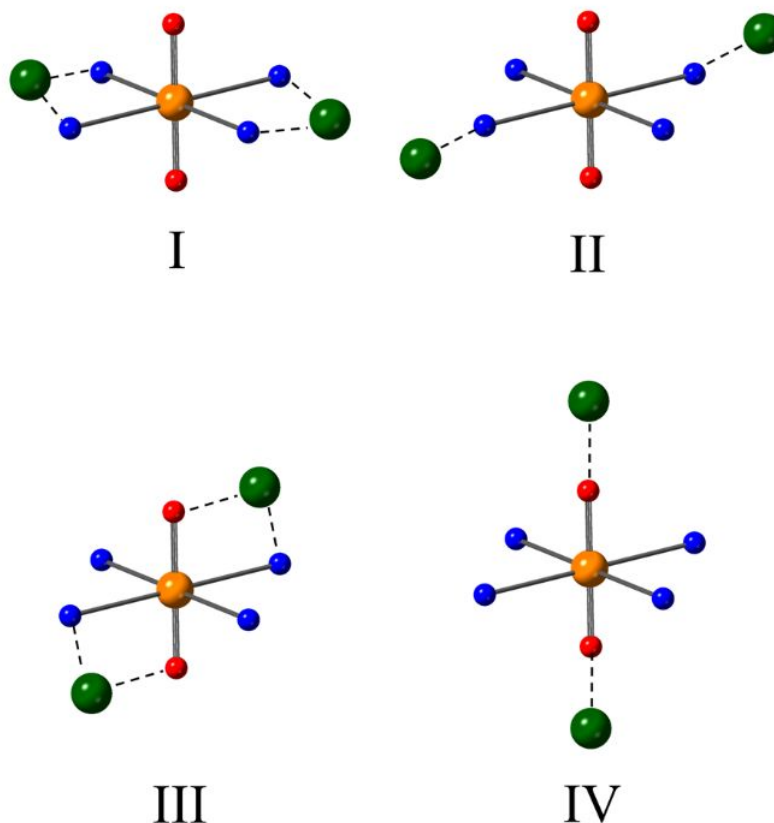
Figure 1. The four possible types of interactions delineated by Danis et al.[19] that occur between alkali cations (Li^+, Na^+, K^+) and $[UO_2X_4]^{2-}$ (X = Cl^-, Br^-). The alkali metal, U, O, and Cl atoms are depicted as green, orange, red, and blue, respectively.

The systematic nature of the Danis *et al.*[19] investigation provides an avenue to continue the exploration of these actinyl-cation interactions with transuranic systems, such as neptunium. These intermolecular interactions with the oxo groups are particularly important for 237-Np because both the NpO_2^+ and NpO_2^{2+} species can be stabilized in solution.[1] Both forms of the neptunyl cation retain the strong bond with the oxo group but the Np=O bond will be weaker in the pentavalent form compared to the hexavalent species. This difference in bond strength can also influence related intermolecular interactions, which in turn can tune the chemical behavior

of the neptunium in solution. Interactions between the NpO_2^+ and low-valent cations (actinyl-cation interaction) has been previously reported in both solution and solid state complex and it is suggested that this type of interaction can influence redox properties, PUREX separation processes and future nuclear fuel reprocessing efforts.[20, 21] There is very little information regarding the extent of these interactions for hexavalent NpO_2^{2+} and additional efforts are needed to document the occurrence of actinyl-cation interactions in both solution and solid phases to further delineate the effects on the chemistry.

The current study builds upon the previous work by Danis *et al.*[19] to explore the interactions of $[NpO_2Cl_4]^{2-}$ complex with alkali cations and systematically investigate the actinyl-cation interactions that occur within these two related systems. Herein, we provide the solid-state structural characterization and Raman spectroscopy of three coordination complexes ((Li(12-crown-4))$_2$[NpO$_2$Cl$_4$] (**LiNp**), (Na(18-crown-6)(H$_2$O))$_2$[NpO$_2$Cl$_4$] (**NaNp**) and (K(18-crown-6))$_2$[NpO$_2$Cl$_4$] (**KNp**)). In addition, we explore actinyl-cation interactions in solution using Raman spectroscopy and provide density functional theory DFT calculations on both the U(VI) and Np(VI) tetrachrolo systems to investigate subtle differences in the actinyl-cation interactions for both species.
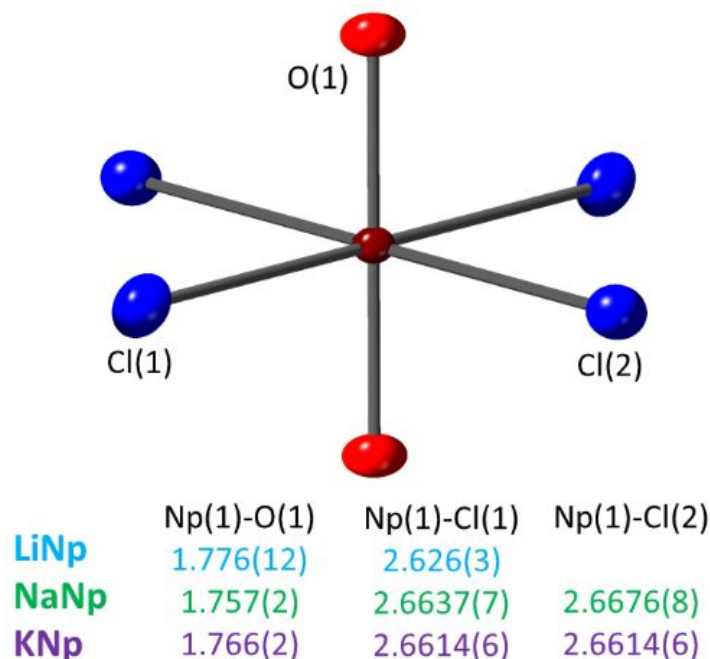
Results

Characterization of Np(VI) chloride system

A series of syntheses for the $[Np(VI)O2Cl_4]^{2-}$ system were developed to evaluate the neptunyl-cation interactions within solid-state coordination compounds. Alkali (Li$^+$, Na$^+$, and K$^+$) chloride salts were combined with crown ether molecules (12-crown-4, 15-crown-5, and 18-crown-6) in a Np(V) or Np(VI) stock solution. Neptunium is a redox active metal and oxidation,

reduction, and disproportionation has been previously observed to occur during room temperature evaporation experiments.[22-24] This phenomenon has been previously observed in the 18-crown-6 system, where reduction of Np(VI) occurs spontaneously in the presence of the crown ether molecule, even in the presence of ozone.[23] We noted that syntheses using Np(V) stock resulted in disproportionation upon evaporation of the solution and the solid product included yellow crystals along with a secondary dark green powder. Two $[Np(VI)O_2Cl_4]^{2-}$ coordination compounds (**NaNp** and **KNp**) were synthesized from room temperature evaporation of the Np(V) aqueous solution and the **LiNp** compound was formed from pure Np(VI) stock solution. We attempted to reproduce the synthesis of **NaNp** and **KNp** with a pure Np(VI) stock solution, but we observed reduction of the Np(VI) to Np(V) and formation of the previously reported $[NpO_2(18\text{-crown-}6)]^+$ complex.[22, 23] All attempts to synthesize materials with the 15-crown-5 ligand were unsuccessful.

Structural characterization of the resulting crystalline material indicated that the coordination geometry about the Np(VI) metal center is a square bipyramid with two short bonds to axial oxygen atoms and four additional Cl⁻ atoms located in the equatorial plane. Np=O bonds within the neptunyl cation are observed at 1.776(12), 1.757(2) and 1.7662(13) Å for **LiNp**, **NaNp**, and **KNp**, respectively (Fig. 2). Np-Cl bond lengths range from 2.614(6) to 2.6676(8) Å. The O=Np=O bond angle is observed in the ideal linear fashion (180°), although there are subtle deviations from 90° for both the O-Np-Cl and Cl-Np-Cl angles for **NaNp** and **KNp**. This variation in intramolecular bond angles is most pronounced within **KNp**, where O-Np-Cl and Cl-Np-Cl angles deviate between 0.48 to 2.97° from the ideal angle of 90°.

	Np(1)-O(1)	Np(1)-Cl(1)	Np(1)-Cl(2)
LiNp	1.776(12)	2.626(3)	
NaNp	1.757(2)	2.6637(7)	2.6676(8)
KNp	1.766(2)	2.6614(6)	2.6614(6)

Figure 2. $[(NpO_2)Cl_4]^{2-}$ coordination complex observed in the **LiNp**, **NaNp**, and **KNp** compounds with Np=O and Np-Cl bond distances determined from analysis by single-crystal X-ray diffraction.

Each of the $[NpO_2Cl_4]^{2-}$ coordination compounds contain charge balancing alkali-cations that are encapsulated within the crown ether molecules (Fig. 3). The Li^+ cation in **LiNp** is encapsulated in the 12-crown-4 molecule and sits at the apical positions of the neptunyl complex (Fig. 3a). Bond distances between the Li^+ cation and the four ether groups range from 2.02(2) to 2.08(1) Å and additional interactions with the neptunyl oxo occurred at distances of 1.92(2) Å. The size of the Na^+ cation in **NaNp** is not ideal for encapsulation within the 18-crown-6 molecule, which results in deviation from a planar geometry and a lowering of the molecular symmetry to a C_2 point group (Fig. 3b). Each Na^+ atom is located near the center of the crown ether with Na-O interatomic distances ranging from 2.486(2) to 2.880(2) Å. An additional water molecule is bound to the Na^+ cation at a distance of 2.355(2) Å and two $[Na(18\text{-crown-}6)(H_2O)]^+$ interact through weak bonds to the a neighboring ether group (O3) at a distance of 2.972(2) Å.

Within the **KNp** compound, the K^+ cation is perched above the 18-crown-6 molecule, with K-O distances ranging from 2.8553(14) to 3.0387(14) Å (Fig. 3c). Additional coordination occurs between the K^+ cation and two Cl^- anions bound to the $[NpO_2Cl_4]^{2-}$ complex at distances of 3.2550(8) and 3.3179(8) Å. These interactions result in a slight puckering of the crown ether to create a lower symmetry C_2 point group associated with the inclusion complex. Overall, the Li^+ cation engages in a Type IV interaction, K^+ cation interacts in a modified Type I motif, and Na^+ cation does not coordinate to the $[NpO_2Cl_4]^{2-}$ complex.
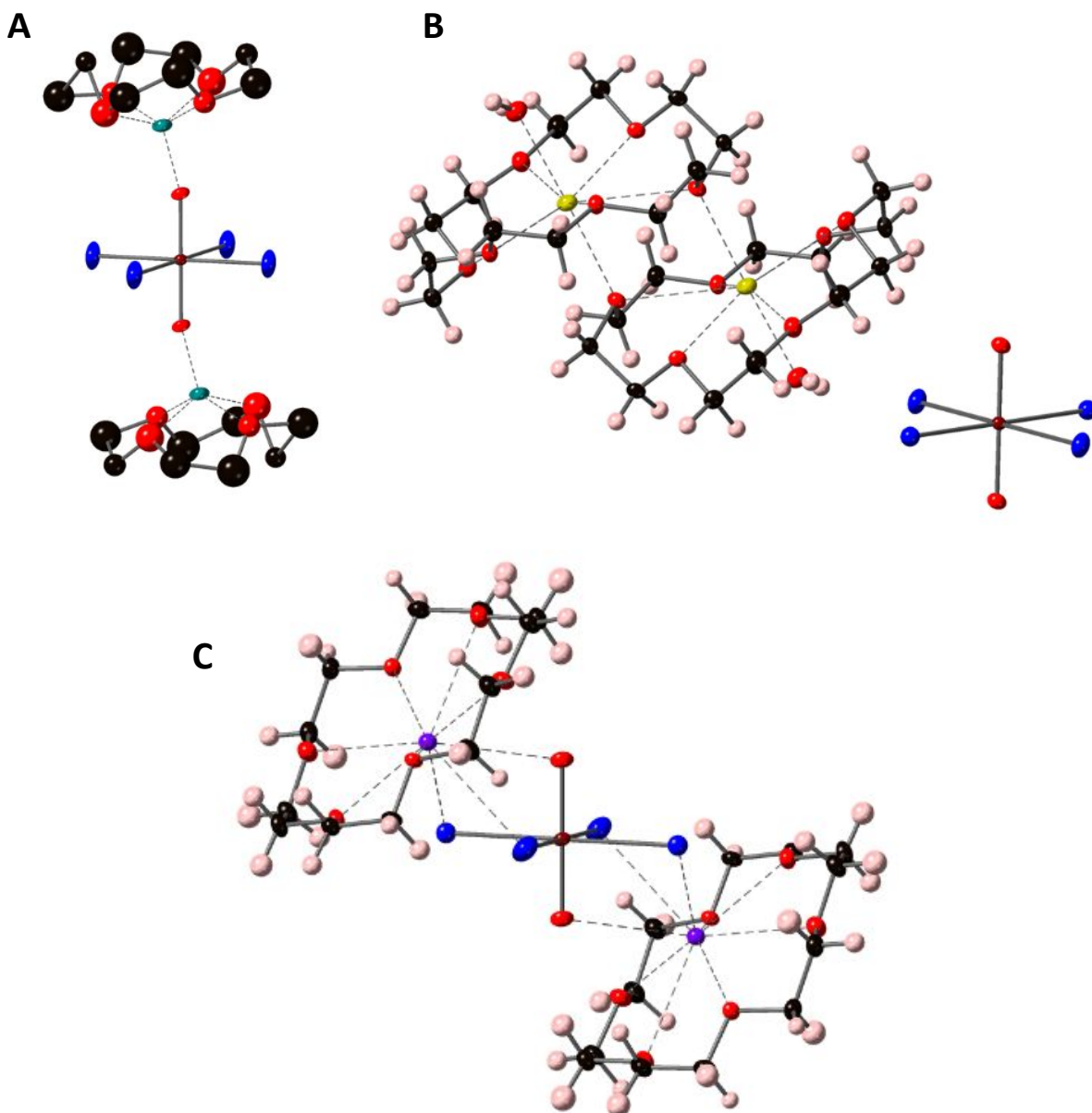
Figure 3. Second sphere coordination between the alkali metal encapsulated within the crown ether molecule and the $[(NpO_2)Cl_4]^{2-}$ complexes for (a) **LiNp**, (b) **NaNp**, and (c) **KNp**. The Np, Cl, O, C, Li, Na, and K atoms are represented by dark red, blue, red, black, teal, yellow and purple ellipsoids, respectively.

Solid-state Raman spectra for all three compounds are complex and exhibit activation of

bands as a result of the lower symmetry crown ether geometry that crystallized within the

coordination compounds. If we define the neptunyl spectral window of interest as occurring

between 790-900 cm^{-1}, then we can identify three to six bands within this region. The spectral

features within the spectral window were fit using a Gaussian non-linear regression fit to

deconvolute the bands and provide peak centroid, full-width half max of the band, and the

tentative spectral assignment. The data are presented in Table 1 and the spectra are located

within the supporting information section.

Table 1. Prominent vibrational bands observed within the Raman spectral window of interest
(800-900 cm^{-1}) for **LiNp**, **NaNp**, and **KNp** compounds.

Peak centroid (cm^{-1})	FWHM (cm^{-1})	Spectral Assignment
LiNp		
793	15.2	ν_1 Np(VI)O$_2$ symmetric stretch
797	7.2	Crown ether ν_{56}
862	8.0	Crown ether ν_{15}
NaNp		
805	15.8	ν_1 Np(VI)O$_2$ symmetric stretch
833	7.6	Crown ether ν_{57}
848	5.1	Crown ether ν_{76}
874	6.8	Crown ether ν_8
896	10.0	Crown ether ν_{37}
KNp		
807	11.9	ν_1 Np(VI)O$_2$ symmetric stretch
830	10.5	Crown ether ν_{71}
859	20	Crown ether ν_{14}
872	8.6	Crown ether ν_8
894	8.0	Crown ether ν_{37}

Complexity of the solid-state Raman spectra provides confirmation that the crown-ether

molecule possesses a lower symmetry conformation. For example, typically the18-crown-6

molecule in a D_{3d} symmetry would only exhibit a medium band at 830 cm^{-1} and a strong

vibrational mode at 870 cm^{-1} within this region.[25] Lowering the symmetry of the crown ether to

C_2 in **KNp** results in activation of additional vibrational modes, which can then be observed in

the Raman spectra. Two bands in the spectral window of interest (797, and 862 cm^{-1}) of **LiNp**

can be assigned to 12-crown-4 modes.[26] The ν_1 symmetric stretch for the neptunyl cation within

[Np(VI)O$_2$Cl$_4$]$^{2-}$ is expected to occur at approximately 800 cm^{-1} based upon characterization of

previously reported compounds.[27]   Therefore, the band at 793, 805, and 807 cm^{-1} have been

assigned to the ν_1 band for **LiNp**, **NaNp**, and **KNp**, respectively.   The FWHM values for the ν_1

NpO$_2$$^{2+}$ bands are slightly larger than those observed for the crown ether molecule (except for the

ν_{14} mode in **KNp**) and are relatively consistent for all three compounds.

Characterization of coordination compounds provide structural and spectral details on the

neptunyl moiety within the solid-state, but these coordination geometries and interactions may

not be fully representative of the conditions in solution. Thus, we turned to solution studies to

further understand the actinyl-cation interactions that may occur within this system.   In the

U(VI) system, the [(UO$_2$)Cl$_4$]$^{2-}$ species is only stable with Cl$^-$ concentrations greater than 12

M.[28, 29]   Solubility limits with NaCl (6.1 M) and KCl (3.76 M) salts do not support the formation

of the [UO$_2$Cl$_4$]$^{2-}$ species; thus, the following Np(VI) solution phase studies could only be

performed for LiCl.

Solution phase Raman experiments with Np(VI) and LiCl.

Raman spectra was collected for 65 mM Np(VI) in 1 M HCl and with five additions of

LiCl solid to create final concentrations of 2.4, 4.8, 7.2 9.6 and 13.3 M Li$^+$ (Figure 4). A broad

band at 856 cm^{-1} was observed in the spectra of the Np(VI) in 1 M HCl. Absence of a band at

767 cm^{-1} or anywhere between 700-800 cm^{-1} indicates that Np(V) is not present and confirms the

purity of the Np(VI) solution. Spectral fitting of the bands present in 1 M HCl specified that the

preferred model was the sum of two Guassian functions with peak centroids located at 857 and

854 cm^{-1} and FWHM of 20.5 and 38.2 cm^{-1}, respectively. Solid LiCl was added the 1 M HCl to create a solution with 2.4 M Li$^+$ and the Raman spectra was collected a second time. The peaks red shifted by 5 cm^{-1} (852 and 849 cm^{-1}) from the original signals, but no significant changes to the FWHM of the peaks was noted in this case. A second addition of LiCl to the solution (total Li$^+$concentration: 4.8 M) caused a further red shift of both bands by an additional 4 cm^{-1}. Increasing the Li$^+$ concentration to 7.2 M resulted in red shift of 11 cm^{-1} for both modes compared to the original signals and the addition of a third peak at 807 cm^{-1}. When the concentration of Li$^+$ cations increased to 9.6 M, the higher frequency band at 842 cm^{-1} was preferentially fit with a single Gaussian function and the band at 807 cm^{-1} increased in intensity. Final addition of LiCl (13.3 M) resulted in an increase in the intensity of the band at 807 cm^{-1} and a stabilization of the band position at 842 cm^{-1}. The intensity ratio between the band at 807 cm^{-1} and 840 cm^{-1} (I_{807}/I_{840}) was calculated at 0.37, 0.44, and 1.47 for the third, fourth, and fifth addition of LiCl salt, respectively.
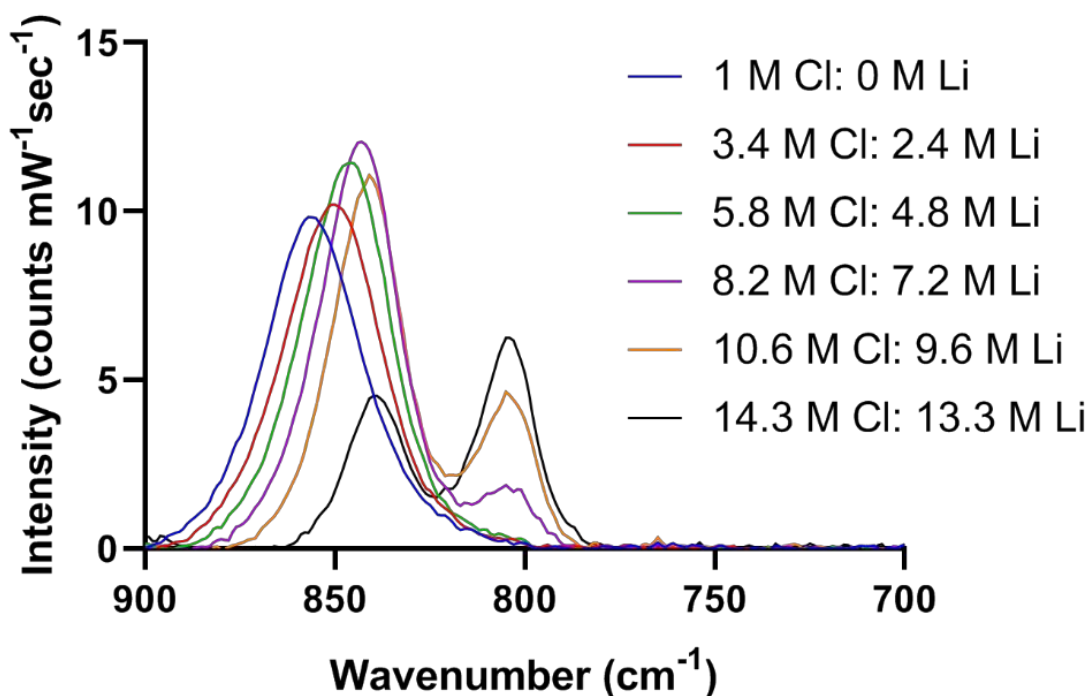
Figure 4. The Raman spectra of Np(VI) in 1 M HCl and with five additions of LiCl solid to create final concentrations of 2.4, 4.8, 7.2 9.6 and 13.3 M Li$^+$

Computational results for Np(VI) interactions with alkali cations

For further analysis of the bands observed in the solution spectra, we turned to DFT calculations for vibrational mode analysis (Table 2). The vibrational analysis of the $[NpO_2Cl_4]^{2-}$ was performed on a structure embedded in a continuum solvent model such that the implicit solvent effects were included in the computed forces along the geometry optimization. A baseline calculation of $[NpO_2Cl_4]^{2-}$ in the absence of any counterions and without imposed symmetry constraints resulted in Np=O and Np-Cl bond lengths of 1.77 Å and 2.68 Å, respectively, which are within 0.02 - 0.03 Å of the **NaNp** and **KNp** solid phases. The ν_1 symmetric stretching vibration for the $[NpO_2Cl_4]^{2-}$ complex without any additional interactions was calculated at 836 cm^{-1}.

Table 2. Relative energy (eV) and calculated vibrational modes (v_1 symmetric stretch and v_3 asymmetric stretch) for the neptunyl cation for the $[NpO_2Cl_4]^{2-}$ complex and related alkali neptunyl chloride complexes for the **KNp**, **NaNp**, and **LiNp** system. The different types refers to previous designation by Danis *et al.*[19] and can be visualized in the supporting information section.

Cation-Type	Relative E (eV)	Calculated v_1 (cm^{-1})	Calculated v_3 (cm^{-1})
$[NpO_2Cl_4]^{2-}$	--	836	916
DFT-KNp			
Type I	-0.24	852	945
Type II	0	845	942
Type III	-0.20	832	925
Type IV	-0.16	835	873
DFT-NaNp			
Type I	-1.82	856	940
Type II	0	830	934
Type III	-1.88	816	902
Type IV	-2.00	864	948
DFT-LiNp			
Type I	0	860	945
Type II	-0.02	857	942
Type III	-0.02	840	925
Type IV	-0.02	809	873

Next, we performed a series of calculations with two Li$^+$ cations arranged in the four different structure types identified by Danis *et al.*[19] Because the crown ethers were not included in the calculated structures, the Li$^+$ cations were fixed at equivalent positions and only the $[NpO_2Cl_4]^{2-}$ molecule was allowed to freely relax in response to the cation interaction (DFT-LiNp). When the Li$^+$ cations solely interact with the Cl$^-$ anions in the equatorial plane (Type I and II), then the Np=O bond distance is calculated at 1.756 Å and the v_1 symmetric stretch is located at 860 and 857 cm^{-1} for DFT-LiNp Type I and Type II interactions, respectively. Positioning the Li$^+$ cation to simultaneously interact with a single Cl$^-$ anion in the equatorial plane and the neptunyl oxo atom (Type III) results in a slight lengthening of the Np=O bond (1.763 Å) and a red shift in the v_1 mode to 840 cm^{-1}. When the Li$^+$ cations only engage in

interactions with the neptunyl oxo (Type IV), then further elongation of the bond (1.80 Å) is observed with an additional red shift in the v_1 stretch to 809 cm^{-1}.   There are only small differences in the relative total energy of these four DFT-LiNp structure types with the highest energy Type 1 structure only +0.029 eV greater than the lowest energy structure (Type III).

While experimentally we are limited by solubility of the alkali salts, computationally we also explore the Na$^+$ and K$^+$ interactions with the [NpO$_2$Cl$_4$]$^{2-}$ complex. Again, the Type I interaction with Na$^+$ cations leads to a Np=O bond distance of 1.756 Å and a v_1 band at 856 cm^{-1}. However, there is a slight elongation of the neptunyl bond (1.771 Å) and red shift (830 cm^{-1}) for the DFT-NaNp Type II structure. DFT-NaNp Type III interactions result in little structural difference in the neptunyl bond compared to Type II, but the v_1 symmetric stretch decreases to 816 cm^{-1}. DFT-NaNp Type IV interactions result in a shorter neptunyl bond distance (1.754 Å) and relatedly the v_1 band blue shifts relative to all the interaction types up to 864 cm^{-1}. The relative differences in total energy for the four DFT-NpNa structure types is much more significant than compared to the DFT-LiNp system. The Type II interaction for Na$^+$ is the highest energy configuration, whereas the type IV is 1.996 eV lower in energy than the Type II. K$^+$ interactions with the [NpO$_2$Cl$_4$]$^{2-}$ complex follow similar trends as observed with the Li$^+$ system, where DFT-KNp Type I and II interactions result in an identical bond distance of 1.758 Å and v_1 bands of 852 and 845 cm^{-1}, respectively. DFT-KNp Type III and IV in the K$^+$ system exhibit minimal elongation (1.77 Å for both), but additional red shift in the spectra (832 and 835 cm^{-1}). For K$^+$ interactions, Type I interactions are the lowest energy state, while Type II is 0.24 eV higher in energy.

Additional computational and experimental evaluation of the U(VI) chloride system

Given the insights gained by the computational study on the $[NpO_2Cl_4]^{2-}$ complex, we extended the DFT study into the $[UO_2Cl_4]^{2-}$ system (Table 3). Initial calculation in the absence of any alkali cations led to distances of 1.79 and 2.69 Å for the U=O and U-Cl bonds, respectively. While the U-Cl bonds are within range of the solid-state structures presented by Danis et al.,[19] the U=O bond is elongated by 0.02-0.03 Å. The uranyl symmetric stretch (v_1) was calculated to be present in the Raman spectra at 841 cm^{-1}, which is similar to bands observed in solid state structures but differs from experimentally derived values obtained in solution by 13 cm^{-1}.[28, 30-32]

Table 3. Relative energy (eV) and calculated vibrational modes (v_1 symmetric stretch and v_3 asymmetric stretch) for the neptunyl cation for the $[UO_2Cl_4]^{2-}$ complex and related alkali neptunyl chloride complexes.

Cation-Type	Relative E (eV)	Calculated v_1 (cm^{-1})	Calculated v_3 (cm^{-1})
$[UO_2Cl_4]^{2-}$	--	841	906
DFT-KU			
Type I	-0.33	855	925
Type II	0	845	918
Type III	-0.19	833	906
Type IV	-0.14	838	910
DFT-NaU			
Type I	-0.06	859	929
Type II	0	854	926
Type III	-0.13	818	889
Type IV	-0.21	865	936
DFT-LiU			
Type I	0	860	930
Type II	-0.04	859	930
Type III	-0.04	841	911
Type IV	-0.13	821	867

The impact of oxo interactions was again explored using DFT calculations for the $[UO_2Cl_4]^{2-}$ complex in the presence of alkali cations with differing orientations (DFT-LiU, DFT-NaU, and DFT-KU). The trends in the calculated bond distances and vibrational modes were

similar to the Np(VI) system, with the most notable difference occurred in the presence of Li$^+$ cations. Bond distances and vibrational modes for Type I, II, and III interactions occurring between Li$^+$ cations and the uranyl oxo are nearly identical to that of the [NpO$_2$Cl$_4$]$^{2-}$species, with subtle differences in the axial bond accounted for based upon actinide size. However, DFT-LiU Type IV interactions do not cause the ν_1 symmetric stretch to red shift as significantly as the neptunyl system, leading to a calculated position of 821 cm^{-1} for the [UO$_2$Cl$_4$]$^{2-}$ complex, compared to 809 cm^{-1} in the case of Np(VI).

The vibrational bands present in uranyl chloride systems have been previously explored experimentally by Nguyen-Trung *et al.* [28] Here, we re-visit this system to provide additional insight into the bands present in these solutions. The high-quality study by Nguyen-Trung *et al.* provides a wealth of knowledge about uranyl speciation and related spectral signals; however, florescence is noted as an issue in the solutions containing high concentrations of LiCl.[28] The previous study utilized a 532 nm excitation source, but we have previously noted that 785 nm lasers can minimize the florescence of the system and improve signal to noise ratios.[33] We initially collected data on UO$_3$ dissolved in 12 M HCl and then after addition of LiCl salt to form solutions containing 5.6 and 11.2 M Li$^+$. Spectral fitting protocols were again utilized to identify the presence of two overlapping bands (843 and 856 cm^{-1}) within the spectra of the 12 M HCl solution. The first addition of LiCl salt to the solution caused a slight blue shift (845 cm^{-1}) in the lower energy peak and a red shift for the second band (854 cm^{-1}) compared to the original spectra obtained in 12 M HCl (Figure 5). Second addition of LiCl solid resulted in a continued blue shift for the first band (847 cm^{-1}), but no significant change in the second peak (855 cm^{-1}). At this point, we reached the solubility limit of the LiCl in 12 M HCl and additional spectra could not be obtained due to the presence of a salt precipitate.[34]
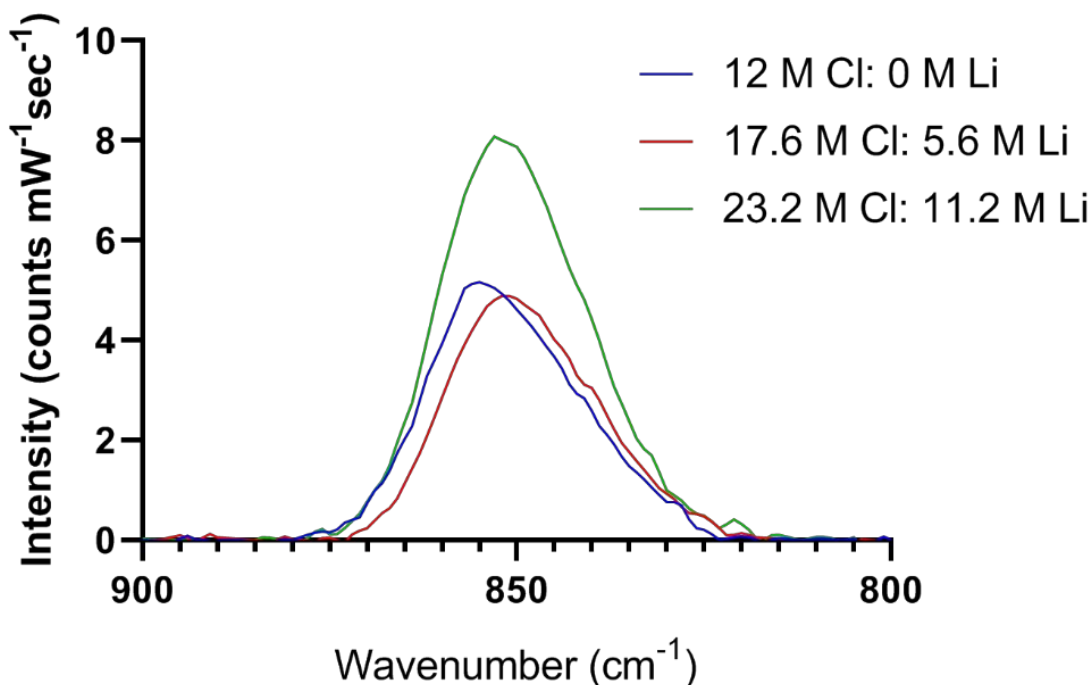
Figure 5. Raman spectra of U(VI) in 12 M HCl with Li^+ concentrations of 5.6 and 11.2 M.

<u>Discussion</u>

Structural features of the $[NpO_2Cl_4]^{2-}$complexes observed in **LiNp**, **NaNp**, and **KNp** are similar to previously reported values.[24, 27, 35] The observed axial bond distances for **NaNp** and **KNp** are consistent with previously reported Np(VI)=O bond distances of 1.752(3) and 1.748(3) Å for $[Ph_3PNH_2]_2[NpO_2Cl_4]$.[24] The neptunyl bond within **LiNp** is elongated to 1.776(12) Å and this is likely due to additional intermolecular interactions with the Li^+ cation. Only one $[Np(V)O_2Cl_4]^{3-}$ complex has previously been crystallized with Np=O bond distances observed at 1.821(4) Å, again suggesting that the neptunium cations in **LiNp**, **NaNp**, and **KNp** are present in the hexavalent oxidation state.[36] Np-Cl bond distances for all three compounds are within range for previously reported tetrachloro species (2.647(1)-2.666(3) Å).[24, 27, 35]

Within the **NaNp** and **KNp** solid-state compounds, the encapsulated alkali cations interact with the $[NpO_2Cl_4]^{2-}$ complex in a different manner than observed interactions in the uranyl system. Within the previously reported uranyl tetrachoro coordination compounds, the Na^+ cation formed two different polymorphs with both Type I (bidentate through the Cl^-) and Type II (monodentate through a single Cl^- anion).[19] For the K^+-$[UO_2Cl_4]^{2-}$ system, only Type I was observed in the resulting solid state coordination compound. As we compare these results to the Np(VI) system, we note that the Na^+ cation does not engage in significant intermolecular interactions with the $[NpO_2Cl_4]^{2-}$ and prefers to interact with a second Na^+-18-crown-6 complex. This is likely due to mismatch in the size of the Na^+ and the ideal cavity volume for the 18-crown-6 molecule prefers this 2:2 form.[37] In the case of K^+, a combined version of type I and II occurs with bidentate interactions between the Cl^- anions on the $[NpO_2Cl_4]^{2-}$ complex and the encapsulated K^+ cation. Unlike the [K(18-crown-6)]$[UO_2Cl_4]$ compound,[19] the K^+ cation is positioned off the equatorial plane of neptunyl complex, leading to additional weak interactions with the neptunyl oxo atom at a distance of 3.47 Å.

Interactions between the Li^+ cation and the $[UO_2Cl_4]^{2-}$ and $[NpO_2Cl_4]^{2-}$ (**LiNp**) complexes are identical.[19] In both cases, a Type IV interaction is observed with sole interactions to the actinyl oxo group. The differences between the interactions of Li^+ and the other alkali cations may be due to the higher charge density associated with the small (0.78 Å) Li^+ cation compared to Na^+ (0.97 Å) and K^+ (1.33 Å) ions. The higher the charge density of the cation, the more likely the actinyl oxo can engage in the electrostatic interactions.

Raman spectra of solid-state compounds are challenging to analyze due to the additional bands from the crown ether molecule. Flexibility of the crown ether can lead to formation of several possible molecular symmetries, which will have different vibrational modes activated in

the Raman spectra. El-Azhary and co-workers published an extensive study that paired DFT calculations with experimental results to determine the variations in the active modes within the vibrational spectra of the 18-crown-6 and 12-crown-4 molecules in different conformations.[25, 26, 38] These studies emphasized the variation that can occur in the Raman spectra of crown ether molecules in different conformations. Also noticeable in the solid-state Raman spectra is the 12-14 cm^{-1} red shift of the ν_1 neptunyl asymmetric stretch in **LiNp**, which is due to the direct interactions with the Li$^+$ cations. The shift in band position also agrees well with the lengthening the Np=O bond to 1.776(12) Å in **LiNp** compared to ~1.75 Å observed in **NaNp** and **KNp**.

Solution studies were performed in the absence of the crown ether molecule to eliminate overlap of the bands and provide additional insight into interactions that may occur in the aqueous phase. The initial Np(VI) stock solution was in 1 M HCl and the two bands are red shifted from the expected ν_1 symmetric stretch assigned to the $[Np(VI)O_2(H_2O)_5]^{2+}$ (863 cm^{-1}) complex,[39] so the two peaks observed in the spectra likely represent $NpO_2Cl_x(H_2O)_y$ species. Under similar conditions in the uranyl system, Nguyen-Trung et al.[28] noted a Cl:U ratio of at least 300 and 700 was needed to support the formation of the $[UO_2Cl]^+$ and $[UO_2Cl_2]^0$ species. The initial stock solution possesses a Cl:U ratio of only 1.5, but the red shift in the Raman spectra does suggest the formation of a hydrated chloro complex. Addition of the LiCl solid leads to further red shifts in the band, suggesting that the number of Cl$^-$ anions bonded to the NpO_2^{2+} increased until reaching a near steady state at 842 cm^{-1}.

The band at 842 cm^{-1} agrees well with the DFT calculation for the Type III interaction with Li$^+$ cations or just with the isolated $[NpO_2Cl_4]^{2-}$ complex. Given the concentration of Li$^+$ in solution, it is likely that some cations inhabit the second sphere coordination environment, thus we will focus on the neptunyl-cation interaction. Type III interaction places the Li$^+$ cation in a

position to bond with both the neptunyl oxo and the Cl$^-$ anion located in the equatorial plane. Calculations indicate that this arrangement represents the lowest energy configuration, although the energy differences between the Type III and the Type II and IV are quite small. In solution, it is possible to have multiple configurations and this may be one of several confirmations that occurs under these conditions.

More surprising was the ingrowth of the band at 807 cm^{-1} with increasing Li$^+$ concentration and our DFT results indicate that this band represents a Type IV interactions between the alkali cation and the neptunyl(VI) oxo. When Li$^+$ is absent from the solution or in lower concentrations, then the band at 809 cm^{-1} is noticeable absent in the Raman spectra. As the concentration of Li$^+$ in solution increases to 7.2 M, then the band begins to emerge and the peak intensity increases with the addition of the LiCl solid. The peak position at 807 cm^{-1} agrees well with the DFT calculated position at 809 cm^{-1} for the Type IV interaction with the Li$^+$ cation. Thus, the Type IV interaction observed in the (Li(12-crown-4)$_2$[NpO$_2$Cl$_4$] solid phase has also been confirmed for the first time in solution.

A similar band within this region had been previously reported in the literature, but it was assigned to the activation of the NpO$_2^+$ asymmetric stretch. Fujii *et al.*[40] utilized Raman spectroscopy to evaluate the spectra of mixed oxidation Np(V/VI) solutions that contained CaCl$_2$ in concentrations that ranged from 3.7 to 6.8 M. In this study, three bands were noted in the Raman spectra at 766-768, 802-805, and 835-839 cm^{-1}. The lowest energy band was assigned to the ν_1 symmetric stretch for the NpO$_2^+$ cation and the peaks between 835-839 cm^{-1} were assigned to the [NpO$_2$Cl$_4$]$^{2-}$ species. Fujii *et al.*[40] assigned the third band at 802-805 cm^{-1} to activation of the ν_3 of the NpO$_2^+$ cation and suggested it was evidence of "cation-cation" or neptunyl(V)-Ca interactions in these solutions. However, recent spectral characterization of a coordination

complex containing neptunyl(V)-Na interaction did not show evidence of ν_3 band activation.[22] Based upon results from this current study, we believe the band at ~803 cm^{-1} observed by Fujii *et al.*[40] is associated with the Ca-neptunyl(VI) interaction, with direct coordination between the Ca^{2+} cation and the neptunyl oxo.

The spectral signals for the U(VI) chloride in the presence of Li$^+$ are different than observed for the Np(VI) chloride system. The band at 856 cm^{-1} agrees well with the presence of the UO$_2$Cl$_3^-$ species (858 cm^{-1}), which is predicted to be the major species at 12 M HCl. Vibrational analysis for UO$_2$Cl$_3$(H$_2$O)$_2^-$ from DFT also calculates the ν_1 symmetric stretching band at 855 cm^{-1}.[28] With additional Cl$^-$ added to the solution, the band shifts to 854 cm^{-1}, which is identical to the band observed for [UO$_2$Cl$_4$]$^{2-}$ by Nguyen-Trung et al[28]. The secondary band at 843 cm^{-1} was unexpected for the 12 M HCl, but not entirely without precedent. A subtle shoulder was previously observed in the spectra obtained when LiCl/U ratios in solution reached 1000-3000, but a high florescence background prevents peak fitting for these conditions.[28] Additional work by Dargent et al.[41] reported an unidentified complex at 841 cm^{-1} with LiCl brines of 8 M. Both Nguyen Trung et al and Dargent et al suggested that this band could be associated with the formation of a soluble polyuranyl chloride species that is connected through bridging Cl$^-$ atoms, but currently there is limited structural evidence of this species occurring in solution.

The experimental values obtained here and in previously reported literature agree well with the DFT calculated vibrational mode at 841 cm^{-1} for a Type III interaction. This suggests that while the Type IV interaction can be stabilized in the solid state, Type III interactions dominates in solution. It is also important to point out that the addition of the crown-ether molecule can influence the overall sterics and the Type IV interaction isolated in solid-state may

in fact be due to the presence of the 12-crown-4 molecule. Thus the differences observed between the solid-state structure and the solution may be influenced by the presence of coordinating ligands. We cannot completely rule out the possibility of a polyuranyl chloride species; however, isolated $[UO_2Cl_4]^{2-}$ complexes have crystallized from multiple high concentration brines. This suggests that we are seeing evidence of a monomeric species with additional interactions from the second sphere Li^+ cations present in solution.[41-49] It is somewhat unclear why we observe the band at 842 cm^{-1} in the concentrated HCl solution, but this peak may be associated with a similar interaction occurring between the oxo and a hydronium cation due to the high acid concentration. Nguyen-Trung also noted that a band at 834 cm^{-1} that occurs in the presence of high tetramethyl ammonium concentrations.[28] Again, the authors suggested the presence of a U(VI) chloro-bridged species, but we currently do not have evidence of this species existing in solution.

While we do not have experimental evidence for the interaction of the K^+ and Na^+ cations in solution, the DFT calculations suggest that limited interactions will occur in these systems. Type I interactions are the lowest energy configuration between K^+ cations and both $[UO_2Cl_4]^{2-}$ and $[NpO_2Cl_4]^{2-}$ complexes and this is also observed in the related solid-state compounds. Multiple interaction may be available for the $[UO_2Cl_4]^{2-}$ and $[NpO_2Cl_4]^{2-}$ species with Na^+ cations. Again, this is borne out in the crystallization of two polymorphs of the (Na(15-crown-5)$_2$[UO$_2$Cl$_4$] material.[19] The lack of direct actinyl-cation interactions for Na^+ and K^+ may be due to the lower charge density compared to the Li^+ cation. Additional studies investigating other higher charge density cations (Mg^{2+} or Ca^{2+}) may provide additional insights into the experimental conditions that would lead to these interactions.

Lastly, it is important to point out that many previous DFT calculations for uranyl and neptunyl systems that report Raman bands typically find differences of 10-60 cm^{-1} experimental and calculated values.[50-52] These differences in the band positions are much larger than the variations of 2-4 cm^{-1} observed in this study. Good agreement observed between vibrational bands observed in experiments and calculated from theory suggests the importance of adding the second sphere coordination environment to the calculations to fully capture the chemical environment of interest. This could be particularly important for high ionic strength solutions and in the presence of counterion that may interact with the actinyl oxo group.

Conclusions

Herein, we presented the synthesis and characterization of three [NpO$_2$Cl$_4$]$^{2-}$complexes crystallized with alkali (Li$^+$, Na$^+$, K$^+$) crown-ether molecules and related solutions. Similar to work by Danis *et al*.,[19] the Li$^+$ cation engaged in direct interactions with the neptunyl oxo, whereas Na$^+$ and K$^+$ cations preferred to coordinate with the Cl$^-$ anions present in the equatorial plane. The solid-state Raman spectra was more complex due to the presence of lower symmetry crown ether molecules, but solution spectra obtained in varying amounts of Li$^+$ cations demonstrated the ingrowth of a vibrational band at 809 cm^{-1} in the Np(VI) solution. Additional DFT calculations indicated that the band arose from direct interactions between the neptunyl oxo groups and Li$^+$ cations (Type IV). Similar experimental and theoretical studies with the [UO$_2$Cl$_4$]$^{2-}$system noted that in solution the Li$^+$ cation likely engages in a Type III interaction instead of the Type IV interaction. The current work demonstrates that high charge density cations will likely engage the U(VI) and Np(VI) actinyl oxo in solution and solid-state structures.

This study has direct implications to speciation, reactivity, and redox behavior of actinyl cations in high ionic strength brines. We have demonstrated in this work that Li^+ cations will directly coordinate to the neptunyl cation, but the previous work by Fujii *et al.*[40], indicates that a similar interaction may occur with Ca^{2+} cations. Oxo interactions with other high charge density cations, such as Mg^{2+}, may also occur and could lead to changes in redox behavior for the system. Additional studies are necessary to evaluate these actinyl-cation interactions in solution and solid-phase system and understand the impact of this second sphere coordination on actinyl chemistry.

Experimental Methods

Synthesis

WARNING: *Neptunium-237 is a highly radioactive alpha emitter and as such is considered a health risk. Research involving this isotope is restricted to specialized laboratories and handled under appropriate regulatory controls and safe working practices.*

Stock Solutions. Approximately 200 mg of ^{237}Np was reprocessed from previous synthetic experiments, precipitated using saturated NaOH, and purified by a cation exchange column containing Dowex-50-X8 resin. Potassium bromate was added to the solution to create the Np(VI) stock solution. The resulting neptunyl (V or VI) hydroxide precipitate was washed three times with ultrapure H_2O and dissolved in 1.0 M HCl. The final concentration of ^{237}Np in each stock solution was determined using a Packard Tri-Carb Liquid Scintillation Counter. The oxidation state of the stock solution was confirmed with absorption and Raman spectroscopy.

LiNp ($[(Li(12-crown-4))_2][NpO_2Cl_4]$): A 1.5mL aliquot of 85mM Np(VI) (1.28 mmol) in 1M HCl was placed into a glass vial. Solid LiCl (0.365g; 8.61 mmol) was added to the vial and

allowed to completely dissolve in the Np(VI) stock solution. A 100 μL aliquot of of this solution was pipetted into a glass crystallization well, followed by addition of 100 μL of a 100mM 12-crown-4 solution to the same well. After 24 hours of slow evaporation dark red crystals formed in good yield.

NaNp ([(Na(18-crown-6)$H_2O)_2$][NpO_2Cl_4]): The solid crystalline material was formed by adding 250μL of 100mM Np(V)O_2 (0.025 mmol) in 1M HCl, 250μL of aqueous 100mM NaCl (0.025 mmol), and 375μL of a 100mM 18-crown-6 (0.038 mmol) aqueous stock solution into a well of a glass crystallization plate. The solution was allowed to evaporate to near dryness over the course of 7 days. A green amorphous powder and yellow (**NaNp**) crystals formed on the bottom of the well.

KNp ([(K(18-crown-6))$_2$][NpO_2Cl_4]): Aliquots of aqueous stock solutions (250μL of 100mM Np(V)O_2 in 1M HCl (0.025 mmol), 250μL of 100 mM KCl (0.025 mmol), and 375 μL of a 100mM 18C6 (0.038 mmol)) were placed directly into a single well of a glass crystallization plate. The solution was allowed to slowly evaporate to near dryness. After 14 days, yellow crystals of KNp and an amorphous green precipitate formed at the bottom of the crystallization well.

Structural Characterization

Suitable single crystals were isolated from their mother liquor and mounted on a MiTeGen cryoloop (d = 50-150 μm) with Paratone-N oil or NVH immersion oil (Cargille Labs). A Bruker D8 Quest single crystal X-ray diffractometer equipped with Mo Kα radiation (λ = 0.71073Å) and an Oxford Systems low temperature cryostream of gaseous N_2 flow operating at

100 K. Data were collected with the Bruker APEX3[53] software package and peak intensities were corrected for Lorentz, polarization, background effects, and absorption using Bruker APEX3 software.[53] The structure solution was determined by intrinsic phasing methods and refined on the basis of F^2 for all unique data using the SHELXTL version 5 series of programs.[54] Np atoms were located by direct methods and the Li, C, O, Na, K, and Cl atoms were found in the difference Fourier maps calculated following refinement of the partial structure models. Hydrogen atoms associated with the 18-crown-6 ligand were fixed using a riding model when possible. Additional information on bond lengths and angles can be found in Tables S1-S3 in the supporting information section and the crystallographic information files can be found on the Cambridge Structural Database by requesting numbers 1912314-1912316.

Several possible unit cells and space groups that could be used to model **LiNp**. Both orthorhombic F and tetragonal I lattices could be identified in the unit cell determination and with the CELL NOW[55] software, but there was no evidence of twinning (over 90% of the reflections could be indexed to either lattice). Unreasonable thermal ellipsoids and more significant disorder of the Li^+ cation and the neptunyl oxo atom was observed when the structure was solved in the tetragonal I (*I4/m* and *I-4*) space groups. Disorder was also observed in the *Fmmm* space group, but more reasonable thermal displacement parameters and bond distances were obtained in this model. Doubling the unit cell parameters independently and solving a lower symmetry space group (*P-1*) did not remove the disorder observed in this structure. Identical issues were observed in [Li(12-crown-4)]$_2$[UO$_2$Cl$_4$] (a = 13.340(1) Å, b = 14.963(1) Å, c = 13.151(1) Å) and could be modeled using either the *Fmm2* or *Fmmm* space groups.[19]

Spectroscopic Characterization

The solid crystalline materials were separated from the mother liquor for analysis by Raman spectroscopy. The crystals were placed in Paratone-N oil to prevent dispersion of the particles. Solutions studies for Np(VI) was performed in a 10mL glass Raman vials fitted with an alumina cap. The spectrum of the initial stock solution was obtained by placing 1.5mL of a 85mM Np(VI) stock solution (1M HCl) into the Raman vial. Solid LiCl salt was added to the solution in four additions: (1) 0.1018 g, (2) 0.1079 g, (3) 0.1094 g, (4) 0.0918 g. The LiCl solid was allowed to fully dissolve before collecting a Raman spectra of the resulting solution. A similar titration study for U(VI), where a stock solution of U(VI) was made by adding 0.10 g of UO_3 to 50mL of concentrated (12N) HCl in a 250 mL glass beaker. A 1.5 mL aliquot of the solution was removed from the beaker and placed into a 10 mL glass vial to collect the Raman spectra. After the spectra was collected, the solution was placed back into the beaker and solid LiCl salt (12.0 g) was added to the solution. The salt was allowed to dissolve before collecting the next Raman spectra. A third Raman spectra was collected after addition of 12.0 g LiCl. The solubility of LiCl in concentrated HCl (~50.4 g/100 mL)[34] limited the subsequent addition of LiCl to this solution.

Both solid-state and solution phase Raman spectra were acquired on a SnRI High-Resolution Sierra 2.0 Raman spectrometer equipped with 785 nm laser energy and 2048 pixels TE-cooled CCD. Laser power was set to the maximum output value of 15 mW and the system was configured to acquire data by the Orbital Raster Scanning mode for solid materials or direct beam for solution, giving the highest achievable spectral resolution of 2 cm^{-1}. Experiments were conducted in dark conditions to mitigate fluorescence interference. Each sample was irradiated for an integration time of 20-60 seconds and automatically reiterated six times in Multi-Acquisition mode. The average of the six Raman spectra acquired for a sample is reported as the

final Raman spectrum. To accurately process the Raman signals observed, the background was subtracted, multiple peaks were fit using the peak analysis protocol with Gaussian functions, and all the fitting parameters converged with a chi-squared tolerance value of 10^{-14} in the OriginPro 9.1.0 (OriginLab, Northampton, MA) 64-bit software. The Raman cross-section for all neptunyl species is assumed to be similar to uranyl, therefore the relative abundance of each species can be estimated using the peak height of the Gaussian function. FWHM values of approximately 5-16 cm^{-1} depending on the nature of the molecular species were considered appropriate for accurate assignment of the spectral bands of the solid-state material. In aqueous solutions, the bands are broader and thus larger values of 15-30 cm^{-1} are considered in the spectral analysis.

Computational Methods

All DFT geometry optimization and vibrational analysis calculations were carried out using the TURBOMOLE program[56] package for *ab initio* electronic structure calculations. Calculations were conducted with the Becke, three parameter, Lee-Yang-Parr (B3-LYP) hybrid functional,[57] using the default polarized split valence (def-SVP) basis set[58, 59] and relativistic effects for U and Np were accounted for using the Stuttgart-type small-core (60 core electrons) relativistic effective core potential (RECPs).[60, 61] Calculations on Np species were spin-polarized. The SCF convergence criterion was set to 0.03 meV, and the geometry optimization was carried out until the forces were converged to at least 5 meV/Å. The initial structure for the $[NpO_2Cl_4]^{2-}$ were obtained from the experimental crystal structures discussed previously and used as input for the geometry optimization. Geometries were allowed to fully relax without any imposed symmetry constraints and using default structural convergence criteria. Aqueous conditions were

simulated using the implicit solvation model COSMO[62] and the water dielectric constant of 78.54.

References

1. L. R. Morss, N. Edelstein, J. Fuger and J. J. Katz, eds., *The Chemistry of the Actinide and Transactinide Elements*, Springer-Verlag Publishing, Berlin, Germany, 2011.
2. P. C. Burns, *Can. Mineral.*, 2005, **43**, 1839-1894.
3. P. C. Burns, R. C. Ewing and F. C. Hawthorne, *Can. Mineral.*, 1997, **35**, 1551-1570.
4. G. Gordon and H. Taube, *J. Inorg. Nucl. Chem.*, 1961, **19**, 189-191.
5. G. Gordon and H. Taube, *J. Inorg. Nucl. Chem.*, 1961, **16**, 272-278.
6. S. A. Gaziev, N. G. Gorshkov, L. G. Mashirov and D. N. Suglobov, *Inorg. Chim. Acta*, 1987, **139**, 345-351.
7. B. J. Masters and S. W. Rabideau, *Inorg. Chem.*, 1963, **2**, 1-&.
8. S. W. Rabideau and B. J. Masters, *J. Phys. Chem.*, 1963, **67**, 318-&.
9. S. W. Rabideau, *J. Phys. Chem.*, 1963, **67**, 2655-&.
10. T. Z. Forbes, C. Wallace and P. C. Burns, *Can. Mineral.*, 2008, **46**, 1623-1645.
11. M. B. Andrews and C. L. Cahill, *Chem. Rev.*, 2013, **113**, 1121-1136.
12. T. Loiseau, I. Mihalcea, N. Henry and C. Volkringer, *Coord. Chem. Rev.*, 2014, **266-267**, 69-109.
13. S. Fortier and T. W. Hayton, *Coord. Chem. Rev.*, 2010, **254**, 197-214.
14. P. L. Arnold, A. F. Pecharman, E. Hollis, A. Yahia, L. Maron, S. Parsons and J. B. Love, *Nat. Chem.*, 2010, **2**, 1056-1061.
15. P. L. Arnold, D. Patel, A. J. Blake, C. Wilson and J. B. Love, *J. Am. Chem. Soc.*, 2006, **128**, 9610-9611.
16. P. L. Arnold, A. J. Blake, C. Wilson and J. B. Love, *Inorg. Chem.*, 2004, **43**, 8206-8208.

17.   C. J. Burns, D. L. Clark, R. J. Donohoe, P. B. Duval, B. L. Scott and C. D. Tait, *Inorg. Chem.*, 2000, **39**, 5464-5468.

18.   P. Thuery and B. Masci, *Dalton Trans.*, 2003, 2411-2417.

19.   J. A. Danis, M. R. Lin, B. L. Scott, B. W. Eichhorn and W. H. Runde, *Inorg. Chem.*, 2001, **40**, 3389-3394.

20.   J. W. Freiderich, A. G. Burn, L. R. Martin, K. L. Nash and A. E. Clark, *Inorg. Chem*, 2017, **56**, 4788-4795.

21.   B. Guillaume, G. M. Begun and R. L. Hahn, *Inorg. Chem*, 1981, **21**, 1159-1166.

22.   M. Basile, E. Cole and T. Z. Forbes, *Inorg. Chem.*, 2018, **57**, 6016-6028.

23.   D. L. Clark, D. W. Keogh, P. D. Palmer, B. L. Scott and C. D. Tait, *Angew. Chem. Int. Ed.*, 1998, **37**, 164-166.

24.   S. M. Cornet, M. P. Redmond, D. Collison, C. A. Sharrad, M. Helliwell and J. Warren, *C. R. Chim.*, 2010, **13**, 832-838.

25.   A. A. Al-Kahtani, N. A. Al-Jallal and A. A. El-Azhary, *Spectrochim. Acta A; Molec. Biomolec. Spectro.*, 2014, **132**, 70-83.

26.   S. Al-Rusaese, A. A. Al-Kahtani and A. A. El-Azhary, *J. Phys. Chem. A*, 2006, **110**, 8676-8687.

27.   D. D. Schnaars and R. E. Wilson, *Inorg. Chem.*, 2018, **57**, 3008-3016.

28.   C. Nguyen-Trung, G. M. Begun and D. A. Palmer, *Inorg. Chem.*, 1992, **31**, 5280-5287.

29.   P. G. Allen, J. J. Bucher, D. K. Shuh, N. M. Edelstein and T. Reich, *Inorg. Chem.*, 1997, **36**, 4676-4683.

30.   D. D. Schnaars and R. E. Wilson, *Inorg. Chem.*, 2014, **53**, 11036-11045.

31.   D. D. Schnaars and R. E. Wilson, *Inorg. Chem.*, 2013, **52**, 14138-14147.

32.   G. Lu, A. J. Haes and T. Z. Forbes, *Coord. Chem. Rev.*, 2018, **374**, 314-344.

33.   G. Lu, T. Z. Forbes and A. J. Haes, *Anal. Chem.*, 2016, **88**, 773-780.

34.   A. Lassin, C. Christov, L. Andre and M. Azaroual, *Am. J. Sci.*, 2015, **315**, 204-256.

35.   M. P. Wilkerson, H. J. Dewey, P. L. Gordon and B. L. Scott, *J. Chem. Crystallogr.*, 2004, **34**, 807-811.

36.   M. K. Payne, M. M. Pyrch, M. Jubinsky, M. C. Basile and T. Z. Forbes, *Chem. Commun.*, 2018, **54**, 10828-10831.

37.   J. W. Steed, *Coord. Chem. Rev.*, 2001, **215**, 171-221.

38.   A. A. El-Azhary and A. A. Al-Kahtani, *Spectrochim. Acta A; Molec. Biomolec. Spectro.*, 2000, **56**, 2783-2787.

39.   L. J. Basile, J. C. Sullivan, J. R. Ferraro and P. Labonville, *Appl. Spectros.*, 1974, **28**, 142-145.

40.   T. Fujii, A. Uehara, Y. Kitatsuji and H. Yamanda, *J. Radioanal. Nucl. Chem.*, 2014, **301**, 293-296.

41.   M. Dargent, J. Dubessy, L. Truche, E. F. Bazarkina, C. Nguyen-Trung and R. Pascal, *Eur. J. Mineral.*, 2013, **25**, 765-775.

42.   N. P. Deifel and C. L. Cahill, *Comp. Rend. Chim.*, 2010, **13**, 747-754.

43.   R. Graziani, G. Bombieri, E. Forsellini and G. Paolucci, *J. Cryst. Molec. Struct.*, 1975, **5**, 1-14.

44.   C. E. Anson, O. AlJowder, U. A. Jayasooriya and A. K. Powell, *Acta Crystallogr. Sect. C-Cryst. Struct. Commun.*, 1996, **52**, 279-281.

45.   R. D. Rogers, A. H. Bond, W. G. Hipple, A. N. Rollins and R. F. Henry, *Inorg. Chem.*, 1991, **30**, 2671-2679.

46.   R. D. Rogers, A. H. Bond and W. G. Hipple, *J. Cryst. Spectros. Res.*, 1990, **20**, 611-616.

47.   M. M. Benning, L. K. Kurihara and R. D. Rogers, *J. Less-Comm. Metals*, 1987, **127**, 269-269.

48.   G. D. Yang and Y. G. Fan, *Sci. China Series B-Chem. Life Sci. Earth Sci.*, 1990, **33**, 1418-1424.

49.   D. J. Watkin, R. G. Denning and K. Prout, *Acta Crystallogr. Sect. C-Cryst. Struct. Commun.*, 1991, **47**, 2517-2519.

50.   T. Fujii, A. Uehara, Y. Kitatsuji and H. Yamana, *J. Radioanal. Nucl. Chem.*, 2015, **303**, 1015-1020.

51.   P. J. Hay, R. L. Martin and G. Schreckenbach, *J. Phys. Chem. A*, 2000, **104**, 6259-6270.

52.   V. Vallet, U. Wahlgren and I. Grenthe, *J. Phys. Chem. A*, 2012, **116**, 12373-12380.

53.   G. M. Sheldrick, *APEX3*, 2015, Bruker AXS, Madison, WI.

54.   G. M. Sheldrick, *Acta Crystallographica Section A: Foundations of Crystallography*, 2008, **64**, 112-122.

55.   Bruker, *CELL NOW a program for unit cell determination*, 2005, Bruker AXS, Madison, WI.

56.   University of Karlsruhe and Forschungszentrum Karlsruhe GmbH *TUROBOMOLE V7.2*. 2017, University of Karlsruhe, Karlsuhe, Germany

57.   A. Becke, *J. Chem. Phys.*, 1993, **98**, 5648-5652.

58.   K. Eichkorn, F. Weigend, O. Treutler and R. Ahlrichs, *Theor. Chem. Acc.*, 1997, **97**, 119-124.

59.   X. D. Cao, M.; Stoll, H. , *J. Chem. Phys.*, 2003, **118**, 487-496.

60.   M. Dolg, in *Theor. Comp. Chem.* 2002, vol. 11, pp. 793-862.

61.   W. Kuchle, M. Dolg, H. Stoll and H. Preuss, *J. Chem. Phys.*, 1997, **100**, 7535-7542.

62.   A. Klamt and G. Schuurmann, *J. Chem. Soc.-Perkin Trans.*, 1993, **5**, 799-805.

TOC Graphic
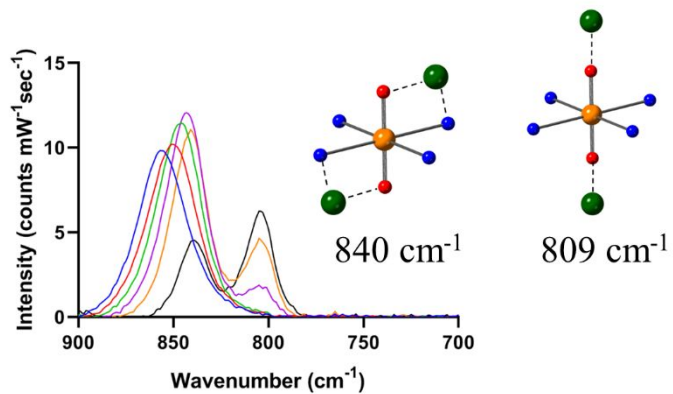
Interactions between the Li$^+$ cation and the neptunyl(VI) oxo observed in both solid state and aqueous solutions.